PCCP

Accepted Manuscript

ROYAL SOCIETY OF CHEMISTRY

www.rsc.org/pccp

Geometric stability and reaction activity of Pt clusters adsorbed graphene substrates for catalytic CO oxidation

Yanan Tang [a,c*], Zhansheng Lu [b], Weiguang Chen [a,c], Wei Li [b] and Xianqi Dai [a,b,c,*]

[a] College of Physics and Electronic Engineering, Zhengzhou Normal University, Zhengzhou, Henan, 450044, People's Republic of China

[b] College of Physics and Electronic Engineering, Henan Normal University, Xinxiang, Henan, 453007, People's Republic of China

[c] Quantum Materials Research Center, Zhengzhou Normal University, Henan 450044, People's Republic of China

Abstract

The geometric stabilities, electronic structures and catalytic properties of tetrahedral Pt_4 clusters anchored on graphene substrates are investigated using the first-principles methods. It is found that the small Pt_4 clusters adsorbed on pristine graphene substrate easily interconvert between structural isomers by the small energy barriers, while the structural interconversion of Pt_4 clusters on the defective graphene and oxygen-doped graphene (O-graphene) have the large energy barriers. Compared to other graphene substrates, the Pt_4 clusters supported on the O-graphene substrate (Pt_4/O-graphene) have the least geometrical distortion and the high symmetry of Pt_4 cluster can enhance the sensitivity of reactive gases. Moreover, the sequential reactions of CO oxidation on the Pt_4/O-graphene are investigated for comparison. Compared with the coadsorption reaction of CO and O_2 molecules, the dissociative adsorption of O_2 as a starting step has a small energy barrier (0.07 eV) and is followed through the Eley-Rideal reaction with an energy barrier of 0.42 eV ($CO + O_{ads} \rightarrow CO_2$). The results provide valuable guidance on fabricating graphene-based catalysis as anode materials, and explore the microscopic mechanism of CO oxidation reaction on atomic-scale catalysts.

*Corresponding author. Tel.:Fax: +86 371 65502273. E-mail address: yntang2010@hotmail.com (Y.N Tang), xqdai@henannu.edu.cn (X.Q. Dai).

1. Introduction

Graphene comprises a two-dimensional (2D) structure of sp^2-hybridized carbon atoms, arranged in a honeycomb crystal lattice.[1] Because of its outstanding electrical,[2] mechanical,[3] and thermal [4] properties, graphene is promising for many potential applications, such as gas sensors,[5] spintronic devices,[6] and transparent electrodes.[7] Especially, graphene nanosheets with huge surface-to-volume ratio can be used as the template to deposit metal atom or clusters.[8-10] Platinum (Pt) is the most efficient catalyst used for fuel cells.[11, 12] The high price and the poor utilization rate of Pt catalysts limit its widely application, thus reduction the particle size is one of the important way to lower the price and enhance the performance of catalyst. By enhancing the catalytically active area relative to the volume of catalysts by using "small clusters," a significantly reduction in consumption is expected. Recently, some results demonstrated that the Pt clusters supported on graphene sheets have high catalytic performances.[13-17]

Characterization and precise control of structural stability and catalytic property of nanoclusters are among the important challenges in the research fields.[18] First, the ligands or the supported substrates can affect the stabilization of nanoclusters and regulate the catalytic reactivity.[19] Second, interactions between nanoclusters and reactant gases will modify the geometric stability and electronic structure of metal clusters.[20, 21] Compared with the unsupported Pt catalysts,[22] the small Pt clusters supported on defective graphene exhibit high stability and chemical activity.[23-25] Therefore, investigations of the structural change in metal clusters supported on different substrates or the gas environments, which is beneficial to understand the stability and catalytic reactivity of metal clusters.

As we known, nanoclusters usually have several structural isomers and the structural change of nanoclusters can effect the concentration of active sites and assist the reactants to overcome reaction barriers.[26] Cuong et al. showed that the Pt clusters on carbon nanotubes (CNTs) exhibit several energetically favored isomers,[27] and the surface curvature can modify the stability and electronic property of Pt clusters.[28] On the pristine graphene (pri-graphene), the metal clusters can easily diffuse and

aggregate to larger structures due to the weak interaction between nanoclusters and substrates.[29] In general, the atom modified graphene can regulate the local configuration, electrons distribution and reactive activity.[30, 31] The bare defects in graphene are inevitably terminated by the oxygen atoms under ambient atmospheres, yet the oxygen-saturated vacancy sites exhibit high reactivity.[32, 33] Therefore, it is highly desirable to explore the existence of oxygen dopant in defective graphene with single vacancy (O-graphene) substrate supported Pt clusters as the electrode materials.

Carbon monoxide (CO) is one of the poisonous and harmful gases in the air and its oxidation is often regarded as an important prototypical reaction for heterogeneous catalytic process.[34] The defect or dopant in graphene acts as nucleation centers or anchoring sites to limit the catalytic nanoparticles growth and improve the stability of metallic catalysts.[35-37] In the current study, the dynamic structural interconversion of Pt clusters, the adsorption behaviors of gas molecules and the reaction mechanisms of CO oxidation on the tetrahedral Pt_4 cluster supported on graphene substrates (Pt_4-graphene) are studied using the first-principles methods. The graphene substrates include the pri-graphene, defective graphene with a single vacancy (SV-graphene) and O-graphene. The Pt_4-graphene can serve as a model to explore graphene-based catalysis in chemical reactions. Moreover, two reaction mechanisms (Eley-Rideal (ER) and Langmuir-Hinshelwood (LH)) will be investigated to clarify the favorable pathways of CO oxidation on the Pt_4/O-graphene substrate. The results would disentangle the factors that effectively control the stability and reactivity of Pt_4 cluster in reaction processes, which is helpful to explore the reaction mechanism on well defined model systems at the atomistic level and provide a valuable reference for designing of graphene-based catalysts.

2. Methods and computational details

The spin-polarized density function theory (DFT) calculations are performed with the Vienna ab initio simulation package (VASP).[38, 39] For improving the calculation efficiency, core electrons are replaced by the projector augmented wave pseudo-potentials[40] and the generalized gradient approximation of Perdew, Burke, and Ernzernhof is used for exchange and correlation.[41] The basis set contained plane

waves with a maximum kinetic energy of 400 eV and the convergence criterion for the electronic self-consistent iteration is set to 10^{-5} eV. The C*2s2p*, Pt*5d6s* and O*2s2p* states are treated explicitly as valence electrons. The calculated lattice constant of graphene is 2.47 Å, which is slightly larger than the experimental value of 2.46 Å.[42] The optimized C-C bonds are 1.43 Å and the graphene supercell is then built based on the calculated lattice constant. The graphene sheet (4×4) is represented using a hexagonal supercell containing 32 carbon atoms. The graphene nanolayer and the adsorbates are free to relax until the self-consistent force drops to below 0.02 eVÅ^{-1}. The distance between the graphene sheet and its images is set to 20 Å, which leads to negligible interactions between the systems and their mirror images. The Brillouin zone integration is sampled using a 5×5×1 Γ-centered Monkhorst-Pack (MP) grid and a Γ-centered MP grid of 15×15×1 is used for the final density of states (DOS) calculations.

Bader charge analysis is used to evaluate the atomic charges and electrons transfer in the reactions.[43] The climbing image nudged elastic band method (CI-NEB) is employed to investigate the saddle points and minimum energy paths (MEPs) for the dissociation or diffusion of reaction gases.[44] The geometric optimization and the search for the transition state (TS) are tested by means of frequency calculations. Six images were inserted into the initial state (IS) or TS and final states (FS) along the MEPs, and the spring force between adjacent images is set to 5.0 eV Å^{-1}. Images are optimized until the forces on each atom are less than 0.02 eVÅ^{-1}. The energy barrier is calculated using the IS as a reference. Calculations of the total energies of a single O atom (or Pt_4 cluster) and gaseous CO, CO_2 and O_2 molecules are performed using periodic cell of 15×15×15 Å^3. The relaxed structures of tetrahedral Pt_4 cluster anchored on the graphene substrates are optimized carefully without any symmetry constraint.

As shown in Fig. 1(a), there are three high symmetric positions on pri-graphene surface, namely the right above a carbon atom (T, the top site), the center of a carbon-carbon bond (B, the bridge site), and the center of the hexagonal carbon ring (H, the hollow site). The tetrahedral Pt_4 cluster anchored on the pri-graphene, the

SV-graphene and the O-graphene supports is denoted as Pt_4/pri-graphene, Pt_4/SV-graphene and Pt_4/O-graphene, respectively. There are three structural isomers of Pt_4 cluster supported on graphene substrates, namely (1) one Pt atom in contacts directly with the graphene labeled configuration 1 (config.1), (2) two Pt atoms in contact directly with the graphene labeled config. 2 and the base of three Pt atoms in contact directly with the graphene labeled config. 3. The gas molecules have been carried out on the possible adsorption sites of Pt_4-graphene surfaces.

The adsorption or coadsorption energy (E_{ads}) of Pt_4 cluster(s) on graphene or gas molecule(s) on a Pt_4-graphene is calculated using the expression:

$$E_{ads} = E_A + E_B - E_{AB} \quad (1),$$

where E_A represents the energies of *A* (Pt_4 cluster, O, O_2, CO and CO_2), E_B represents the total energies of *B* (the pri-, SV- and O-graphene or Pt_4-graphene), and E_{AB} represents the total energies of *AB* (graphene systems with adsorbates).

3. Results and discussion

3.1. Geometric stability and structural interconversion

The reported geometrical rule of stable clusters found three highest symmetric clusters with 4, 6, 12 atoms and that with 4 atoms has the tetrahedral structure.[45] In addition, the previous results reported that tetrahedral Pt_4 cluster is the most stable configuration on graphene substrates as compared with the dimer Pt_2, triangle Pt_3, linear or quadrilateral Pt_4.[46-48] However, few reports provide systemic information about the dynamical structural interconversion between the supported metal clusters on various graphene substrates and the structural change of metal clusters under ambient conditions, which are needed in order to understand the catalytic behavior of nanoclusters during reaction processes.

From the energy point of view, the most stable configuration has the largest adsorption energy. We investigate the relaxed structures of the Pt_4 clusters on three graphene substrates by setting up various initial structures, and three stable configuration of Pt_4-graphene systems are shown in Fig. 1(b)-(d), including the config.2 of Pt_4/pri-graphene with adsorption energies (E_{ads}, 3.08 eV), the config.1 of

Pt_4/SV-graphene (4.36 eV) and the config.3 of Pt_4/O-graphene (3.74 eV). In contrast to pri-graphene and O-graphene substrates, the Pt_4 cluster anchored on SV-graphene has the largest adsorption energy, where one Pt atom in Pt_4 cluster interacts with dangling bonds of carbon atoms around the vacancy site. The Pt atoms contacting with the pri-graphene (or O-graphene) substrate are preferably adsorbed at the bridge sites or top sites of C atoms, which is in accordance with the adsorption of single Pt atom on graphene.[49, 50]

The adsorption of Pt_4 cluster induces the structural distortion of graphene surfaces. For the Pt_4/SV-graphene, the height of carbon atom nearby the Pt1 atom is drawn out by 0.65 Å, which likely changes some of the sp^2-like character to a more covalently reactive sp^3-like character. In addition, the competitive effects between Pt-C and Pt-Pt interactions, the tetrahedral geometry of Pt_4 clusters are slightly distorted as compared with the free-tetrahedral Pt_4 cluster (2.64 Å), namely the Pt-Pt bonds vary from 2.55 to 2.67 Å on the pri-graphene, the SV-graphene (2.50 ~ 2.68 Å) and the O-graphene (2.58 ~ 2.65 Å). It is found that the Pt_4 clusters have the least structural distortion on the O-graphene as compared with the other Pt_4-graphene systems.

As shown in Table. 1, the small energy differences indicate that the adsorbed Pt_4 clusters on graphene substrates can easily interconvert between their isomers at low temperature. In the next section, we will discuss the structural interconversion of three configurations of Pt_4 clusters on graphene substrates. For the Pt_4 clusters anchored on the pri-graphene, the structures and energy barriers for interconversion pathways between these configurations are shown in Fig. 2(a). Passing over a TS1 (0.18 eV), one of the upper atoms in Pt_4 cluster (config.1) falls to the graphene surface and then form the config.2. To proceed, the config.2 directly converts into the config.3 through the TS2 with a large energy barrier (0.42 eV). In addition, it is difficult to convert from configs.3 and 2 to config.1 because of the relatively large energy barriers (0.43 and 0.48 eV). In comparison, the configs.1 and 3 can easily convert into the config.2 through the small energy barriers (0.18 and 0.20 eV). This result means that the config.2 of Pt_4 cluster is the most stable on the pri-graphene.

The interconversion pathways and energy barriers for the adsorbed Pt_4 clusters on the SV-graphene are shown in Fig. 2(b). The energy barriers between isomers vary from 0.37 to 3.18 eV. Firstly, one of the upper atoms in Pt_4 cluster (config.1) falls to the graphene surface, then the config. 1 converts into config.2 (TS1) with a large energy barrier of 3.18 eV. It is found that the conversion pathways through and TS1 (0.37 eV) and TS3 (0.53 eV) have the low-energy barriers, illustrating that the Pt_4 cluster can easily interconvert from configs.2 and 3 to config.1, so the config.1 of Pt_4 cluster is the most stable on the SV-graphene.[23, 51]

Before the Pt_4 isomers supported on the O-graphene, we investigate the structural stability of O-graphene sheet. It is found that the large adsorption energy of O dopant in the graphene layer (7.40 eV) and it nearly retains the planar form of graphene (with the dopant height of 0.07 Å), indicating that the O-graphene sheet would be stable enough to be used as substrate. Then, the interconversion pathways between these Pt_4 isomers on the O-graphene are shown in Fig. 2(c), and the corresponding energy barriers vary from 0.13 to 0.93 eV. The structural conversion from config.1 to config.2 goes through the TS1 with a slightly small barrier of 0.21 eV. To proceed, the conversion pathway from config.2 to config.3 has much smaller energy barrier (0.13 eV) than the config.3 conversion into config.1 (0.93 eV). In all, the interconversion reactions from configs.1 and 2 to the config.3 have quite small energy barriers (0.17 and 0.13 eV), indicating the config.3 of Pt_4 cluster is the high capability and stability on the O-graphene.

It is found that the small adsorption energies and barriers of Pt_4 isomers on the pri-graphene suggest that the Pt_4 clusters easily interconvert and may coalescence into large clusters. Thus, it is hard to experimentally achieve the dispersion of small Pt clusters on the pri-graphene support. The large adsorption energies and barriers of Pt_4 clusters on the SV-graphene and O-graphene substrates imply that the Pt_4 clusters are rather stable and thus facilitate the dispersion of Pt clusters.[24, 52, 53] In addition, the Pt_4 clusters anchored on the O-graphene (or the SV-graphene) have the least (or largest) structural distortion and flexibility. The above results illustrate that the structural introversion and stability of Pt_4 clusters can be modulated by the different graphene

substrates, which allows us to study the adsorption behaviors of nanoclusters on graphene nanosheets.

3.2. Electronic structure of Pt_4-graphene systems

Electronic structure is directly related to the interaction between adsorbate and substrate, which fundamentally determine the physical and chemical properties of a system. Herein, we investigate the charge density difference (CDD) of three stable configurations of Pt_4-graphene systems, and the corresponding contour lines in plots are drawn at 0.041 e/Å^3 intervals. As shown in Fig. 3(a)-(c), it is found that electrons deplete from the vicinity of the Pt-Pt bonds and accumulate in the vicinity of the Pt-C interfaces. The more pronounced charge density distribution between the Pt_4 clusters and the SV-graphene (or O-graphene) indicates that the strong interaction between adsorbed Pt_4 clusters and graphene substrates. Comparatively, there is small charge density accumulation between Pt_4 cluster and pri-graphene interface. Because the defective structure and the O dopant in graphene can induce the structural distortion of graphene surface and promote the local charge redistribution, resulting in the enhancement of the substrate-adsorbate interaction.

To gain more insight into the origin of the stability of Pt_4 anchored on graphene substrates, we investigate the DOS plots of the Pt_4-graphene systems, as shown in Fig. S1. Compared with the bare graphene systems, the broadened partial DOS (PDOS) of Pt_4 5*d* states overlapped with the total DOS (TDOS) states of systems around the Fermi level (E_F), suggesting the strong hybridization between the Pt atoms and graphene substrate. According to the symmetry of spin channels, the non-magnetic property of pri-graphene and O-graphene convert into the magnetic materials when the Pt_4 cluster is adsorbed. As shown in Fig. S2, it is clearly shown that the *d*-band width of the Pt_4 cluster is broadened and reduced on the SV-graphene as compared with those on the pri-graphene and O-graphene. According to the *d*-band centers (ε_d) analysis,[54] the Pt_4/pri-graphene and Pt_4/O-graphene close to the E_F (ε_d= −1.82 eV and −1.79 eV), while the *d*-band centers of the Pt_4/SV-graphene moves away from the E_F (ε_d= −2.73 eV) due to the more electrons are transferred from Pt_4 cluster to the SV-graphene.[25, 55]

Using Bader charge analysis,[43] it is found that more electrons (*e*) are transferred from the Pt_4 cluster to the SV-graphene (0.46 *e*) than that on the pri-graphene (0.23 *e*) and O-graphene (0.27 *e*). The Pt2 and Pt3 atom loses 0.23 and 0.20 *e* in the Pt_4/pri-graphene, the Pt1 atom loses 0.70 *e* in the Pt_4/SV-graphene and the Pt1, Pt2 and Pt3 atom loses 0.10, 0.23 and 0.13 *e* in the Pt_4/O-graphene. So, the different positions of atoms in Pt_4 cluster can exhibit the positively or negatively charged, which may regulate the active sites of Pt_4 cluster toward the reactants.[25, 56] In addition, the transferred electrons help us to explain the change in magnetic property of graphene systems by the adsorbed Pt_4 clusters, since electrons which are spin polarized in the Pt_4 cluster are transferred to the less polarized graphene states.[57] On the other hand, we have checked the effect of spin-orbit coupling (SOC) on the results of adsorption energies and magnetic moments, and the calculated results are shown in Table 1. It is found that, by including the SOC, the adsorption energies of Pt_4 clusters on three graphene substrates are relatively decreased. However, the most stable configuration of Pt_4 clusters are not changed as compared with the other isomers. In addition, these structural isomers of Pt_4 clusters also induce the change in magnetic property of systems. These results indicate that the energy difference between structural isomers depends on the change in magnetic moment. The SOC has effects on the adsorption energy and magnetic moment to some extent, but it does not affect the most preferable adsorption structures of the Pt_4 clusters.

3.3. Adsorption of gas molecules on Pt_4-graphene

Based on the most stable configuration of Pt_4-graphene substrates, the adsorption of gas molecule (O_2 and CO) is carried out on three high symmetric sites of Pt_4 cluster, namely the T site directly above the Pt atom, the B site at the midpoint of the Pt-Pt bond, the H site at the center of the Pt-Pt-Pt triangle, and the possible adsorption sites and energies are listed in Table 2. The structural stability of Pt_4 clusters under the gas environment and the adsorption behaviors of reactants on the Pt_4-graphene is a vital issue to clarify the microscopic mechanism of CO oxidation reactions.[58]

Firstly, we investigate the site-selected adsorption of gas molecules on the Pt_4/pri-graphene (config. 2). As shown in Table 2, the end-on configuration of CO on

the T site of Pt1 atom has the largest adsorption energy (2.08 eV) than that on other T sides (Pt2 1.83 eV and Pt4 1.88 eV), B site (Pt1-P4, 1.68 eV) and H site (Pt1-Pt2-Pt4, 1.37 eV). The distance between CO and Pt1 is 1.85 Å, the C-O bond length is elongated to 1.17 Å and the Pt1 is drawn out by 0.19 Å. For the adsorption of O_2 molecule, the most stable configuration is characterized by O_2 paralleled to the T site of Pt1 atom with E_{ads} of 1.28 eV, which is more favorable than that on the T site of Pt4 (1.14 eV) and parallel to the Pt1-Pt4 bond (0.98 eV). The O-O bond length is elongated to 1.36 Å and the Pt1 atom is drawn out by 0.37 Å. Although the O_2 is parallel to the Pt1-Pt2 and Pt2-Pt4 bonds with the large E_{ads} of 2.53 and 2.55 eV, yet the adsorbed O_2 induce a great structural distortion of Pt_4 cluster, where two base Pt atoms (Pt2 and Pt3) are perpendicularly adsorbed on pri-graphene and the tetrahedral Pt_4 cluster convert into the quadrilateral structure. This result means that the config.2 of Pt_4/pri-graphene has less endurance and easily experiences the structural distortion under the gas O_2 environments.

For the adsorption of gas molecules (CO and O_2) on the Pt_4/SV-graphene (config.1), the configuration (end-on) of CO on the T site of Pt3 atom (2.59 eV) is more stable than that on other T sites (Pt2 1.84 eV and Pt4 2.08 eV), B site (Pt3-Pt4, 1.53eV) and H site (Pt2-Pt3-Pt4, 1.25 eV), as shown in Table. 2. The C-O bond length is elongated to 1.17 Å and the neighboring Pt3 atom is drawn out by 0.48 Å. In addition, the O_2 paralleling to the T site of Pt3 atom (1.60 eV) is more stable than that on the T site of Pt4 atom (1.52 eV) and paralleling to the Pt3-Pt4 (1.30 eV). The neighboring Pt3 atom is drawn out by 0.28 Å and the O-O bond is elongated to 1.36 Å. It is found that the adsorbed O_2 is parallel to the Pt1-Pt3 and Pt2-Pt4 bond with large adsorption energies (2.16 and 2.43 eV) and also induce a structural distortion of Pt_4 cluster, namely the tetrahedral Pt_4 cluster converted into the quadrilateral structure and the base Pt1 atom embedded into the SV site. Hence, the config.1 of Pt_4/SV-graphene has less endurance under the O_2 gas environment.

For the Pt_4/O-graphene system (config. 3), the most energetically favorable configurations of the gas molecules and the corresponding DOS plots are shown in Figs. 4 and 5. The end-on configuration is favourable for the CO at the T site of Pt4

atom (2.04 eV), which is more stable than that on the T site of Pt1 atom (1.80 eV), the B site of Pt1-Pt4 bond (1.75 eV) and the H site of Pt1-Pt3-Pt4 (1.45 eV). Meanwhile, there are about 0.32 electrons are transferred from Pt_4/O-graphene to CO, which occupies the CO-$2\pi^*$ states and leads to the elongation of the C-O bond to 1.17 Å. The Pt4-CO distance is 1.84 Å and their intersection angle is 179.5°, indicating that the CO is vertically adsorbed on the T site of Pt4 atom, as shown in Fig. 4(a). The strong hybridization between PDOS of Pt *5d* states and the $2\pi^*$, 5σ states of CO is observed around the E_F, as shown in Fig. 5(a). This indicates that the variation in bond strength is caused by CO-Pt coupling. In addition, the symmetric spin channels indicate that the adsorbed CO on Pt_4/O-graphene exhibits the non-magnetic property (zero u_B).

The most energetically favourable configuration for O_2 on the Pt_4/O-graphene is shown in Fig. 4(b). The adsorbed O_2 is parallel to the Pt1-Pt4 bond (1.55 eV) with the largest adsorption energy than the B site of Pt1-Pt4 bond (1.26 eV) and the T site of Pt4 atom (1.33 eV). There are about 0.70 electrons are transferred from the Pt_4/O-graphene to O_2, which occupy the $2\pi^*$ orbital of O_2 and subsequently lead to the elongation of the O-O bond to 1.44 Å. The O_2 molecule is possible dissociative through the more elongated O-O bond, which may facilitate the CO oxidation reaction. Figure 5(b) shows that electrons mainly accumulate on O_2 and makes the O_2 $2\pi^*$ orbital half-filled. The broadened PDOS of Pt *5d* states strongly hybridize with O_2 $2\pi^*$ and 5σ orbital around the E_F and also overlap with the TDOS. In addition, the hybridization between Pt and O atoms induce the magnetic moment of the whole system (2.0 u_B). Hence, the magnetic character of Pt_4-graphene system can be regulated by the gas molecules.[59] Noting that the adsorption of O_2 molecule can not induce the structural distortion of Pt_4 cluster on O-graphene.

It is concluded that the stability of gas molecules is obviously varied according to the structural isomer of Pt_4 clusters. Compared with the Pt_4/pri-graphene and Pt_4/SV-graphene, there is less structural distortion of Pt_4 clusters supported on the O-graphene under the O_2 gas environment. This means that the O-graphene can be used as the ideal substrate for supported nanoclusters. The adsorption energy and geometry are determined not only by the cluster itself, but also by the supported

materials and other environmental conditions. Compared to other Pt_4-graphene substrates, the reactive gases have the moderate energies and small energy difference on the Pt_4/O-graphene, which may promote their interaction in the catalytic reaction. Therefore, the study allows us to understand the specific reaction mechanism including the relationship between the adsorption energy and energy barrier, existing within the reactive gases and the Pt_4/O-graphene.

4.4. CO oxidation reaction on Pt_4/O-graphene

There are two well-established reaction mechanisms (the LH and ER) for the adsorbed CO and O_2.[23, 60, 61] The LH mechanism involves the coadsorption of CO and O_2 molecules reacts with each other (IS), the formation of a peroxo-type O-O-C-O complex as intermediate state (MS). In the final state (FS), a CO_2 molecule is released and leaving a chemisorbed atomic O (O_{ads}) adsorbs on the catalysts. For the ER mechanism, the gas-phase CO molecule directly approaches the preadsorbed O_2 molecule. Based on the calculated results, the elongate bond of O_2 prefers to choose the dissociative reaction as a starting step and is followed by the ER reaction (CO + O $\rightarrow$ CO_2). In addition, the adsorption of an O_{ads} and CO_2 at the T sites of Pt4 atom has an E_{ads} of 5.08 and 0.05 eV. In our study, two mechanisms (ER and LH) for the sequential CO oxidation reaction on the Pt_4/O-graphene are investigated for comparison.

For the ER reaction, the atomic configurations at each state along the reaction pathways are displayed in the Fig. 6(a), and the corresponding structural parameters for IS, TS and FS are shown in Table 3(a). Firstly, the most stable configuration of O_2 is parallel to the Pt1-Pt4 bond as an IS, the corresponding distance between O1-O2, O1-Pt4 and O2-Pt1 is 1.44, 1.97 and 1.95 Å, respectively. To proceed, two oxygen atoms within O_2 start to approach the neighboring Pt atoms and the system reaches the TS. The energy barrier of the TS is estimated to be 0.07 eV, where the bond distances between O1-O2, O1-Pt4 and O2-Pt1 is 1.71, 1.88 and 1.87 Å, respectively. Passing over the TS, the O-O bond is broken and both bond distances of O1-Pt4 and O2-Pt1 are 1.77 Å. Secondly, we check whether the formed atomic O_{ads} is active for CO oxidation through the ER reaction, as shown in Fig. 6(a). The configuration with a CO

molecule more than 3.0 Å away from the preadsorbed O1 on the Pt4 atom is viewed as an IS2. The FS2 is set to the configuration with a CO_2 adsorbs on the Pt4 atom and leaving another O2 anchors on the Pt1 atom. When the carbon atom of CO approach to the O1, a TS2 with the CO-O1 distance of 1.81 Å is formed and the process goes through the ER reaction with an energy barrier of 0.42 eV. Thirdly, the leaving O2 atom diffuses from Pt1 atom to Pt4 atom, and the corresponding diffusion pathways and energy barriers are shown in Fig. 6(b). The IS and FS is set to the configuration with the O2 atom anchors at the Pt1 and Pt4 atom, and the center site of Pt1-Pt4 bond is viewed as the MS, the corresponding structural parameters are shown in Table 3(b). The single O2 atom diffuses from IS to MS and then moves to FS, and the corresponding energy barrier is 0.63 and 0.73 eV, respectively. Finally, the single O2 atom on the Pt4 atom reacts with the physisorbed CO through the ER reaction (0.51 eV), as shown in Fig. 6(b). The generating CO_2 molecule can easily desorb from the reactive site due to its small adsorption energy. It is found that the formation of first CO_2 through ER reaction has a smaller energy barrier (0.42 eV) than the formation of second CO_2 (0.51 eV). Compared with the previous works,[62, 63] the CO oxidation reactions on the Pt_4/O-graphene have the relatively smaller energy barriers than those of commonly used Pt catalysts (> 1.0 eV).

As an important reference, the coadsorption of CO and O_2 on the Pt_4/O-graphene through the LH reaction are investigated. The corresponding structural parameters for CO oxidation (IS, TS, MS and FS) are shown in Table 3(c). The configuration of the CO molecule is tilted to the Pt4 atom and the adsorbed O_2 is parallel to the Pt1-Pt4 bond as an IS, as shown in Fig. 6(c). The bond length of CO and O_2 is 1.16 and 1.36 Å, and the Pt4-CO and Pt4-O_2 distance is 1.85 and 2.28 Å, respectively. To proceed, one of the oxygen atoms (O1) in the O_2 molecule starts to approach the carbon atom of CO and the system reaches the TS, the corresponding reaction has the large energy barrier of 1.11 eV. Passing over the TS, a peroxo-type O-O-C-O complex (MS) is formed and the corresponding O1-O2 bond is elongated from 1.36 to 1.58 Å. The reaction achieve from the MS to the FS without any energy barrier, where the O1-O2 bond is broken and a CO_2 molecule is formed, leaving an atomic O2 adsorbs on the

Pt1 atom. Then, the O2 atom diffuses from Pt1 to Pt4 and reacts with the CO molecule through the ER reaction, as shown in Fig. 6(b). Compared with the dissociative adsorption of O_2 molecule, the formation of OOCO complex through the LH reaction has the large energy barriers (1.11 eV), suggesting the LH reaction as a starting step is hardly possible on the Pt_4/O-graphene. Hence, the sequential reactions of CO oxidation on the Pt_4/O-graphene include a two step processes: the dissociative adsorption of O_2 and is followed by the ER reaction ($CO + O_{ads} \rightarrow CO_2$). This result is different from the LH reaction on the single Pt anchored graphene,[31, 55] since there are more active sites in the Pt_4 cluster than the single-atom Pt catalyst.

In light of the aforementioned discussions, it is concluded that the adsorption stability and catalytic activity of the supported Pt_4 clusters can be modulated by different graphene substrates. Compared with the pri-graphene and SV-graphene substrates, the O-graphene can effectively prevent the structural distortion of Pt_4 cluster under the gas environments and reduce the site-selected adsorption for reactive gases. Moreover, the CO oxidation reactions on the Pt_4/O-graphene have small energy barriers and are likely to proceed rapidly in the practical catalytic reaction, which provide a valuable method to fabricate the functionalized graphene with low-cost and high catalytic efficiency.

4. Conclusion

The geometric stability and catalytic properties of Pt_4-graphene systems are studied using the first-principles methods. It is found that the adsorption energies and interconversion barriers of Pt_4 cluster on the SV-graphene and O-graphene are larger than that on the pri-graphene. Compared with the pri-graphene and SV-graphene substrates, the Pt_4 cluster supported on O-graphene (config. 3) can effectively prevent the structural distortion under O_2 gas environment and the high symmetry of Pt_4 cluster can improve the sensitivity for reactive gases. For the CO oxidation reactions, the dissociative adsorption of O_2 as an initial reaction is energetically favorable on the Pt_4/O-graphene and is followed through the ER reaction ($CO + O_{ads} \rightarrow CO_2$). These results provide beneficial reference to stimulate the applications of graphene-metal composite catalysis, and improve the efficiency and stability of carbon-based anode

materials.

Acknowledgments

This work was supported by the National Natural Science Foundation of China (Grant No.U1404109, 51401078 and 11247012), and the Science Fund of Educational Department of Henan Province (Grant No. 14B140019, 14A140015 and 14A140010). The authors are grateful to Ruifeng Lu for suggestions and revision of the manuscript.

Supplementary Information

Fig.S1. Spin-resolved total DOS (TDOS) and the partial DOS (PDOS) (spin-up labeled with ↑ and spin-down labeled with ↓) for Pt_4 cluster on the (a) pri-graphene, (b) SV-graphene and (c) O-graphene, respectively. The solid, dashed and dotted lines represent the TDOS of graphene without (with) Pt_4 clusters and the PDOS of Pt_4 cluster *5d* states. The vertical dotted line denotes the Fermi level.

Fig.S2. The *d*-bond DOS plots and the corresponding *d*-bond centers (ε_d), respectively. The solid, dashed and dotted lines represent of Pt_4 cluster anchored on the (a) pri-graphene, (b) SV-graphene and (c) O-graphene, respectively. The vertical dotted line denotes the Fermi level.

References

1 A. Geim and K. Novoselov, *Nat. Mater.*, 2007, **6**, 183-191.

2 M. Orlita, C. Faugeras, P. Plochocka, P. Neugebauer, G. Martinez, D. K. Maude, A. L. Barra, M. Sprinkle, C. Berger, W. A. de Heer and M. Potemski, *Phys. Rev. Lett.*, 2008, **101**, 267601.

3 C. Lee, X. Wei, J. W. Kysar and J. Hone, *Science*, 2008, **321**, 385-388.

4 A. A. Balandin, S. Ghosh, W. Bao, I. Calizo, D. Teweldebrhan, F. Miao and C. N. Lau, *Nano Lett.*, 2008, **8**, 902-907.

5 Y. H. Zhang, Y. B. Chen, K. G. Zhou, C. H. Liu, J. Zeng, H. L. Zhang and Y. Peng, *Nanotechnology*, 2009, **20**, 185504.

6 N. Tombros, C. Jozsa, M. Popinciuc, H. Jonkman and B. Van Wees, *Nature*, 2007, **448**, 571-574.

7 K. S. Kim, Y. Zhao, H. Jang, S. Y. Lee, J. M. Kim, J. H. Ahn, P. Kim, J. Y. Choi and B. H. Hong, *Nature*, 2009, **457**, 706-710.

8 G. Williams, B. Seger and P. Kamat, *ACS Nano*, 2008, **2**, 1487-1491.

9 G. M. Scheuermann, L. Rumi, P. Steurer, W. Bannwarth and R. Mulhaupt, *J. Am. Chem. Soc.*, 2009, **131**, 8262-8270.

10 B. Seger and P. Kamat, *J. Phys. Chem. C*, 2009, **113**, 7990-7995.

11 A. Bell, *Science*, 2003, **299**, 1688-1691.

12 F. Raimondi, G. Scherer, R. Koetz and A. Wokaun, *Angew. Chem. Int. Ed.*, 2005, **44**, 2190-2209.

13 R. Siburian and J. Nakamura, *J. Phys. Chem. C*, 2012, **116**, 22947-22953.

14 P. Blonski and J. Hafner, *J. Chem. Phys.*, 2011, **134**, 154705.

15 O. Zengi Aktrk and M. Tomak, *Phys. Rev. B*, 2009, **80**, 85417.

16 E. Yoo, T. Okata, T. Akita, M. Kohyama, J. Nakamura and I. Honma, *Nano Lett.*, 2009, **9**, 2255-2259.

17 E. Yoo, T. Okada, T. Akita, M. Kohyama, I. Honma and J. Nakamura, *J. Power Sources*, 2011, **196**, 110-115.

18 D. Astruc, F. Lu and J. Aranzaes, *Angew. Chem. Int. Ed.*, 2005, **44**, 7852-7872.

19 C. T. Campbell, *Nat. Chem.*, 2012, **4**, 597-598.

20 I. Fampiou and A. Ramasubramaniam, *J. Phys. Chem. C*, 2013, **117**, 19927-19933.

21 D. H. Lim and J. Wilcox, *J. Phys. Chem. C*, 2011, **115**, 22742-22747.

22 S. Proch, M. Wirth, H. S. White and S. L. Anderson, *J. Am. Chem. Soc.*, 2013, **135**, 3073-3086.

23 M. Zhou, A. Zhang, Z. Dai, C. Zhang and Y. Feng, *J. Chem. Phys.*, 2010, **132**, 194704.

24 G. Kim and S. H. Jhi, *ACS nano*, 2011, **5**, 805-810.

25 Y. N. Tang, Z. X. Yang and X. Q. Dai, *J. Nanopart. Res.*, 2012, **14**, 844.

26 N. Tian, Z. Y. Zhou, S. G. Sun, Y. Ding and Z. L. Wang, *Science*, 2007, **316**, 732-735.

27 N. Cuong, A. Sugiyama, A. Fujiwara, T. Mitani and D. Chi, *Phys. Rev. B*, 2009, **79**, 235417.

28 H. C. Dam, N. T. Cuong, A. Sugiyama, T. Ozaki, A. Fujiwara, T. Mitani and S. Okada, *Phys. Rev. B*, 2009, **79**, 115426.

29 D. Chi, N. Cuong, N. Tuan, Y. Kim, H. Bao, T. Mitani, T. Ozaki and H. Nagao, *Chem. Phys. Lett.*, 2006, **432**, 213-217.

30 Q. Tang, Z. Zhou and Z. Chen, *Nanoscale*, 2013, **5**, 4541-4583.

31 Y. N. Tang, Z. X. Yang, X. Q. Dai, D. W. Ma and Z. M. Fu, *J. Phys. Chem. C*, 2013, **117**, 5258-5268.

32 Y. N. Tang, X. Q. Dai, Z. X. Yang, L. J. Pan, W. G. Chen, D. W. Ma and Z. S. Lu, *Phys. Chem. Chem. Phys.*, 2014, **16**, 7887-7895.

33 J. M. Carlsson, F. Hanke, S. Linic and M. Scheffler, *Phys. Rev. Lett.*, 2009, **102**, 166104.
34 H. J. Freund, G. Meijer, M. Scheffler, R. Schlogl and M. Wolf, *Angew. Chem. Int. Ed.*, 2011, **50**, 10064-10094.
35 Y. N. Tang, Z. X. Yang and X. Q. Dai, *J. Nanosci. Nanotechnol.*, 2013, **13**, 1612-1615.
36 M. N. Groves, C. Malardier-Jugroot and M. Jugroot, *J. Phys. Chem. C*, 2012, **116**, 10548-10556.
37 B. Xiong, Y. Zhou, Y. Zhao, J. Wang, X. Chen, R. O'Hayre and Z. Shao, *Carbon*, 2013, **52**, 181-192.
38 G. Kresse and J. Furthmüller, *Comput. Mater. Sci.*, 1996, **6**, 15-50.
39 G. Kresse and J. Furthmüller, *Phys. Rev. B*, 1996, **54**, 11169-11186.
40 G. Kresse and D. Joubert, *Phys. Rev. B*, 1999, **59**, 1758-1775.
41 J. Perdew, K. Burke and M. Ernzerhof, *Phys. Rev. Lett.*, 1996, **77**, 3865-3868.
42 J. Carlsson and M. Scheffler, *Phys. Rev. Lett.*, 2006, **96**, 46806.
43 G. Henkelman, A. Arnaldsson and H. Jónsson, *Comput. Mater. Sci.*, 2006, **36**, 354-360.
44 G. Henkelman, B. Uberuaga and H. Jónsson, *J. Chem. Phys.*, 2000, **113**, 9901-9904.
45 G. Meng, N. Arkus, M. P. Brenner and V. N. Manoharan, *Science*, 2010, **327**, 560.
46 K. Okazaki-Maeda, Y. Morikawa, S. Tanaka and M. Kohyama, *Surf. Sci.*, 2010, **604**, 144-154.
47 X. Q. Dai, Y. N. Tang, J. H. Zhao and Y. W. Dai, *J. Phys: Condens. Matter*, 2010, **22**, 316005.
48 X. Q. Dai, Y. N. Tang, Y. W. Dai, Y. H. Li, J. H. Zhao, B. Zhao and Z. X. Yang, *Chin. Phys. B*, 2011, **20**, 056801.
49 Y. N. Tang, Z. X. Yang and X. Q. Dai, *J. Magn. Magn. Mater.*, 2011, **323**, 2441-2447.
50 Y. N. Tang, Z. X. Yang and X. Q. Dai, *J. Chem. Phys.*, 2011, **135**, 224704.
51 M. J. Lopez, I. Cabria and J. A. Alonso, *J. Phys. Chem. C*, 2014, **118**, 5081-5090.
52 T. Kondo, T. Suzuki and J. Nakamura, *J. Phys. Chem. Lett.*, 2011, **2**, 577-580.
53 Y. Li, W. Gao, L. Ci, C. Wang and P. M. Ajayan, *Carbon*, 2010, **48**, 1124-1130.
54 B. Hammer and J. K. Nørskov, *Adv. Catal.*, 2000, **45**, 71-129.
55 Y. N. Tang, Z. X. Yang and X. Q. Dai, *Phys. Chem. Chem. Phys.*, 2012, **14**, 16566-16572.
56 S. Funk, U. Burghaus, B. White, S. O'Brien and N. Turro, *Top. Catal*, 2007, **44**, 145.
57 B. Uchoa, C. Lin and A. Castro Neto, *Phys. Rev. B*, 2008, **77**, 035420.
58 G. Somorjai, *Surf. Sci.*, 1979, **89**, 496-524.
59 Y. N. Tang, X. Q. Dai, Z. X. Yang, Z. Y. Liu, L. J. Pan, D. W. Ma and Z. S. Lu, *Carbon*, 2014, **71**, 139-149.
60 Y. Li, Z. Zhou, G. Yu, W. Chen and Z. Chen, *J. Phys. Chem. C*, 2010, **114**, 6250-6254.
61 E. H. Song, Z. Wen and Q. Jiang, *J. Phys. Chem. C*, 2011, **115**, 3678-3683.
62 A. Alavi, P. Hu, T. Deutsch, P. L. Silvestrelli and J. Hutter, *Phys. Rev. Lett.*, 1998, **80**, 3650-3653.
63 M. Ackermann, T. Pedersen, B. Hendriksen, O. Robach, S. Bobaru, I. Popa, C. Quiros, H. Kim, B. Hammer, S. Ferrer and J. W. M. Frenken, *Phys. Rev. Lett.*, 2005, **95**, 255505.

Table.1. The adsorption energies (E_{ads}, eV) and magnetic moments (m, μ_B) for the Pt_4 clusters (including the config.1, config.2 and config.3) supported on three graphene substates (without and with SOC).

Systems		Pt_4/pri-gra		Pt_4/SV-gra		Pt_4/O-gra	
		E_{ads}	m	E_{ads}	m	E_{ads}	m
Without SOC	Config.1	2.91	1.80	4.36	1.86	3.39	1.86
	Config.2	3.08	1.90	3.68	1.68	3.43	1.63
	Config.3	2.96	1.70	3.86	1.14	3.74	1.48
With SOC	Config.1	2.71	1.90	4.20	0.98	3.20	2.55
	Config.2	2.88	2.60	3.54	1.99	3.28	1.88
	Config.3	2.79	0.95	3.85	1.01	3.64	0.85

Table.2. The adsorption energy (E_{ads}) of CO and O_2 molecules on three Pt_4-graphene systems, the corresponding adsorption sites including the top (T), the bridge (B) and the hollow (H) sites.

System	Pt_4/pri-gra (config.2)			Pt_4/SV-gra (config.1)			Pt_4/O-gra (config.3)		
Sites	$T_{(Pt1)}$	$B_{(Pt1-Pt4)}$	$H_{(Pt1-Pt2-Pt4)}$	$T_{(Pt3)}$	$B_{(Pt3-Pt4)}$	$H_{(Pt2-Pt3-Pt4)}$	$T_{(Pt4)}$	$B_{(Pt1-Pt4)}$	$H_{(Pt1-Pt3-Pt4)}$
CO	2.08	1.68	1.37	2.59	1.53	1.25	2.04	1.75	1.45
Sites	$T_{(Pt1)}$	$T_{(Pt4)}$	$T_{(Pt1-Pt4)}$	$T_{(Pt3)}$	$T_{(Pt2-Pt4)}$	$T_{(Pt3-Pt4)}$	$T_{(Pt1-Pt4)}$	$T_{(Pt4)}$	$T_{(Pt1-Pt3)}$
O_2	1.28	1.14	2.55	1.60	2.43	1.30	1.55	1.33	0.79

Table.3. Structural parameters of the CO oxidation on the Pt_4/O-graphene, (a) the dissociation of O_2 and CO + O → CO_2 reaction, (b) a single O_{ads} diffuses from Pt1 to Pt4 and CO + O → CO_2 reaction, and (c) CO + O_2 → OOCO → CO_2 + O_{ads}, IS, TS, MS and FS are displayed in Figs. 8 (a), (b) and (c).

(a)	IS	TS	FS
d_{Pt4-O1}	1.97	1.88	1.77
d_{Pt1-O2}	1.95	1.87	1.77
d_{O1-O2}	1.44	1.71	5.05
	IS1	TS2	FS2
d_{Pt4-O1}	1.77	1.82	2.69
d_{C-O1}	3.28	1.81	1.18
d_{C-O}	1.14	1.16	1.17

(b)	IS	MS	FS
d_{Pt1-O2}	1.80	1.99	4.04
d_{Pt4-O2}	3.69	1.90	1.77
	IS2	TS2	FS2
d_{Pt4-O2}	1.77	1.84	2.17
d_{C-O2}	3.03	1.78	1.26
d_{C-O}	1.15	1.16	1.20

(c)	IS	TS	MS	FS
d_{C-O}	1.16	1.17	1.22	1.25
d_{C-Pt4}	1.85	1.93	1.97	2.12
d_{Pt4-O1}	2.28	3.13	2.99	3.06
d_{O1-O2}	1.36	1.35	1.58	3.86
d_{Pt1-O2}	1.94	1.94	1.89	1.77

Figure captions

Fig.1. Schematic illustrating (a) the three high symmetry sites: the hollow (H), the top (T) and the bridge (B) on graphene surface. The while and red sphere denotes the single vacancy (SV) and the O dopant, the indices of the Pt atoms are shown within the adsorbed Pt_4 clusters. The most stable configuration of Pt_4 clusters on (b) the pri-graphene, (c) the SV-graphene and (d) the O-graphene substrate. The red, black and gray balls represent O, C and Pt atoms, respective.

Fig.2. Structural interconversion and energy barriers for the Pt_4 cluster isomers from the configurations 1 to 3 on the (a) pri-graphene, (b) SV-graphene and (c) O-graphene. The red, black and gray balls represent O, C and Pt atoms, respectively.

Fig.3. The valence charge density difference plots of Pt_4 clusters on the (a) pri-graphene, (b) SV-graphene and (c) O-graphene, respectively. Contour lines in plots are drawn at about 0.041 e/Å^3 intervals, and the solid (dashed) lines denote the charge accumulation (depletion).

Fig.4. Top and side views of the geometric structure for the (a) CO and (b) O_2 adsorbed on the Pt_4/O-graphene. Red, black and white balls represent O, C and Pt atoms, respectively.

Fig.5. Spin-resolved TDOS, local DOS (LDOS), PDOS (spin-up labeled with ↑ and spin-down labeled with ↓) for (a) CO and (b) O_2 on Pt_4/O-graphene. The solid and dash dotted curves represent the TDOS of Pt_4/O-graphene with CO (or O_2) adsorption and the PDOS of Pt4 *5d* states with CO (or O_2) adsorption, and the dashed curves represents the LDOS of adsorbed CO (or O_2). The vertical dotted line denotes the Fermi level.

Fig.6. The minimum energy profiles and the configurations of different states for CO oxidation reactions on Pt_4/O-graphene, including (a) the dissociation of O_2 and CO + O_{ads} reaction, (b) the diffusion of O_{ads} and CO + O_{ads} reaction, (c) the CO + O_2 reaction. Red, black, and white balls represent O, C and Pt atoms, respectively.

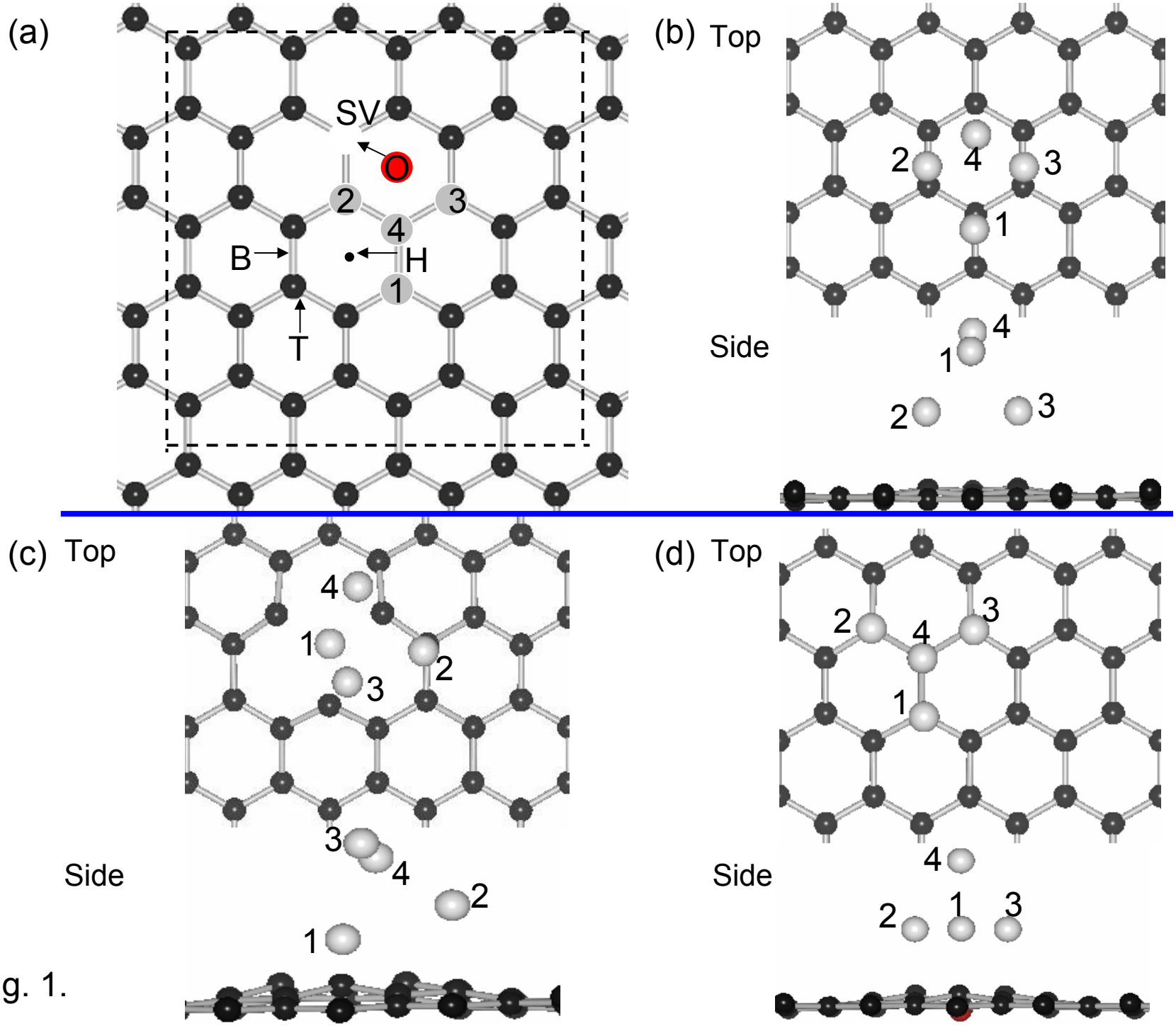

Fig. 1.

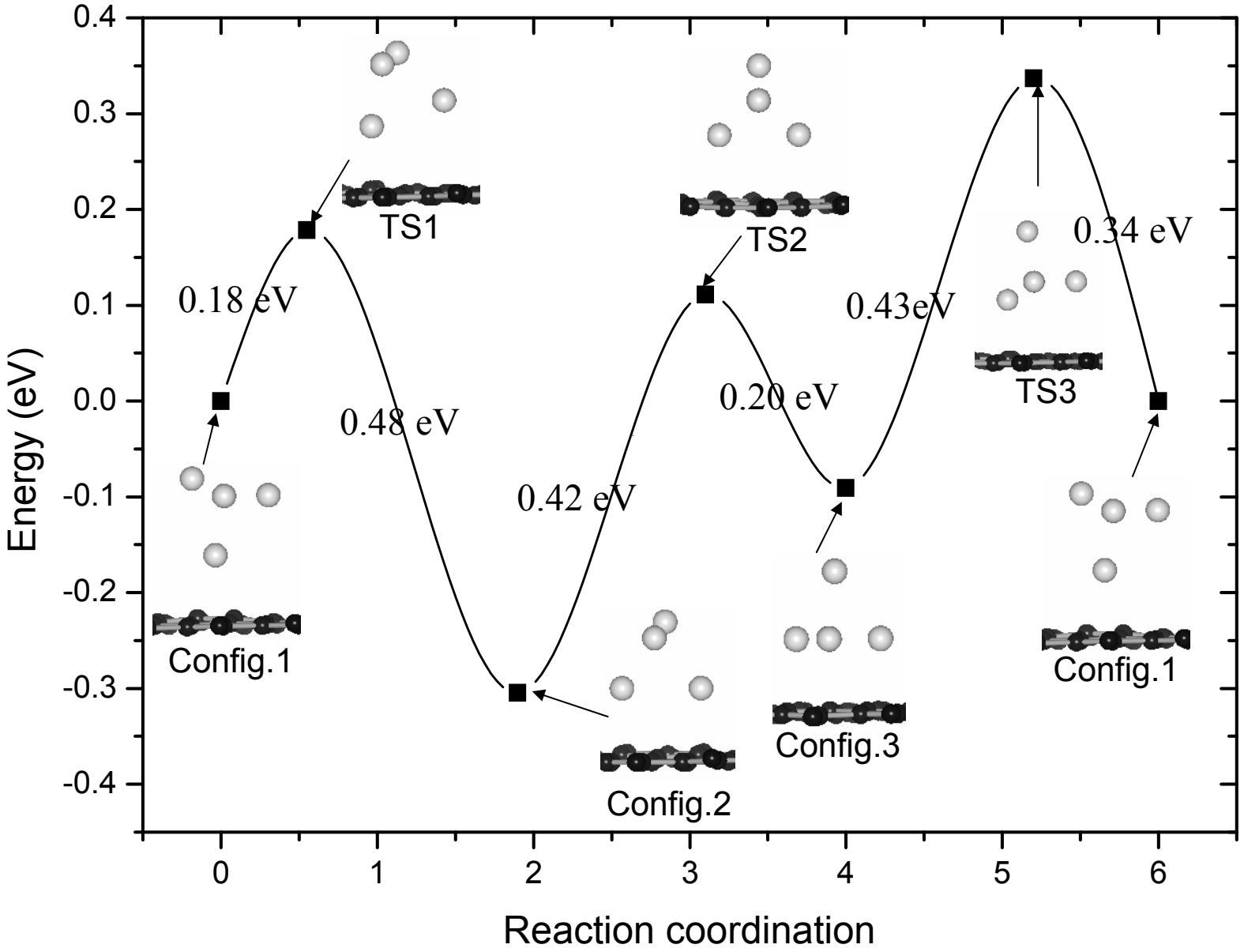

Fig. 2(a)

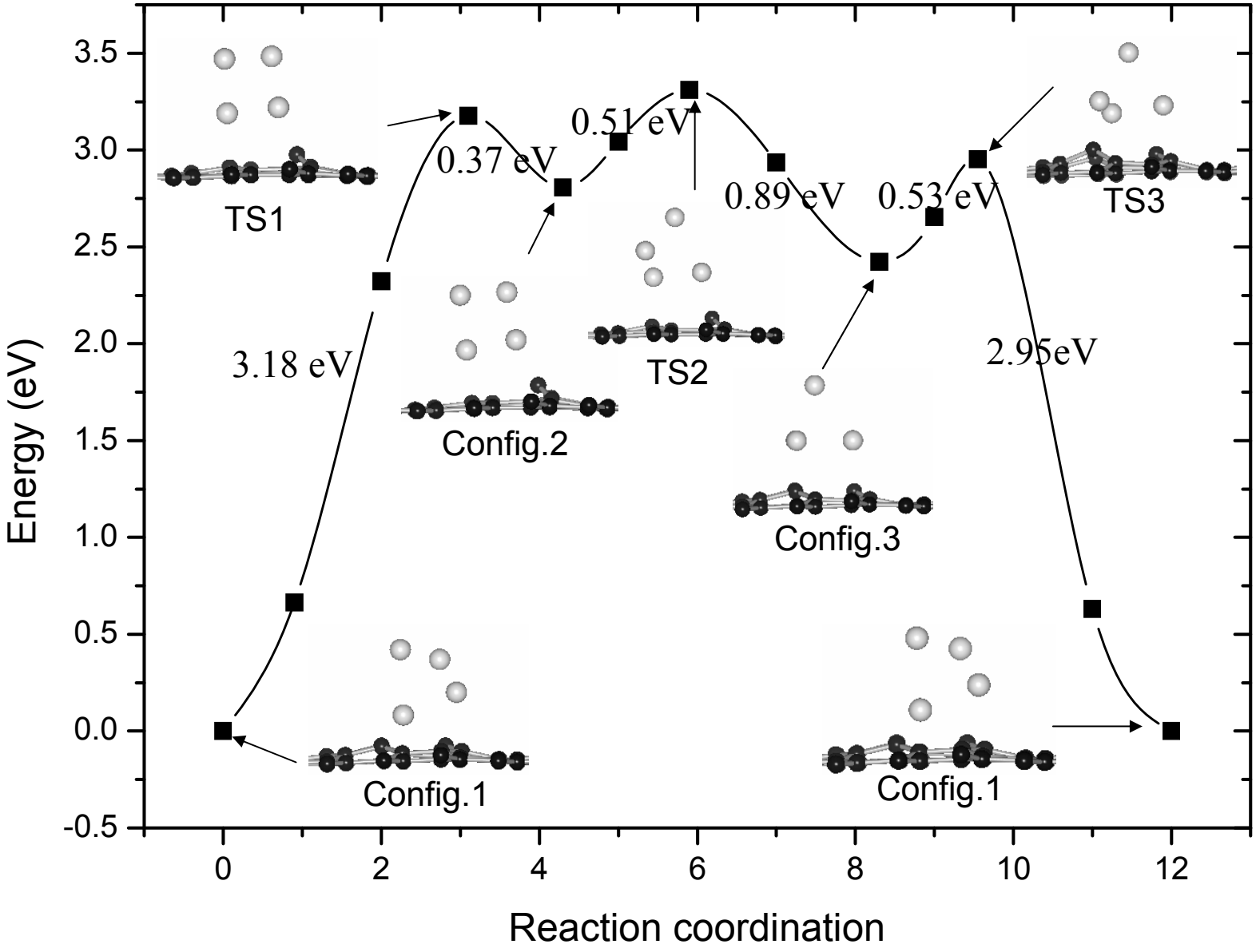

Fig. 2(b)

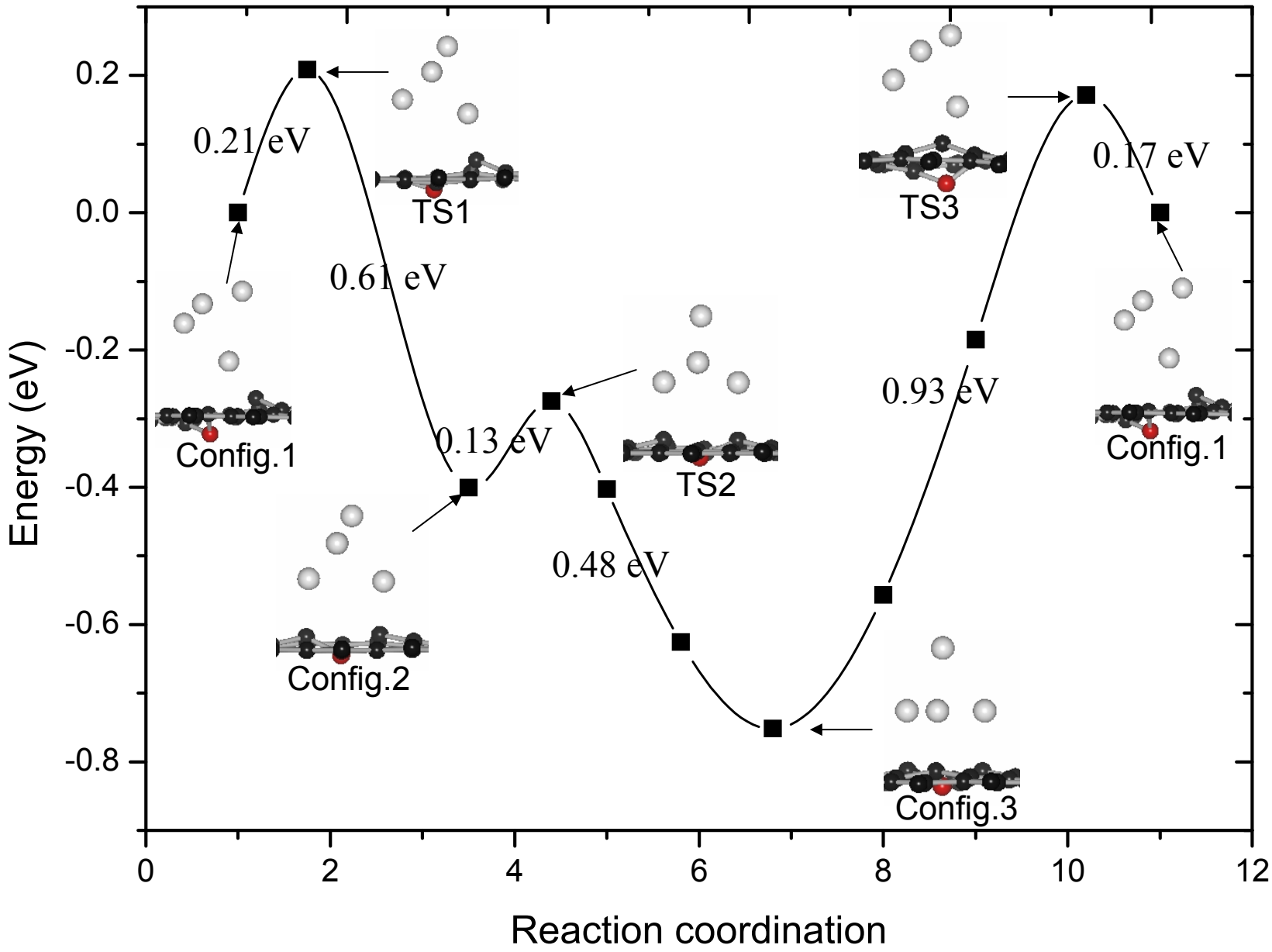

Fig. 2(c)

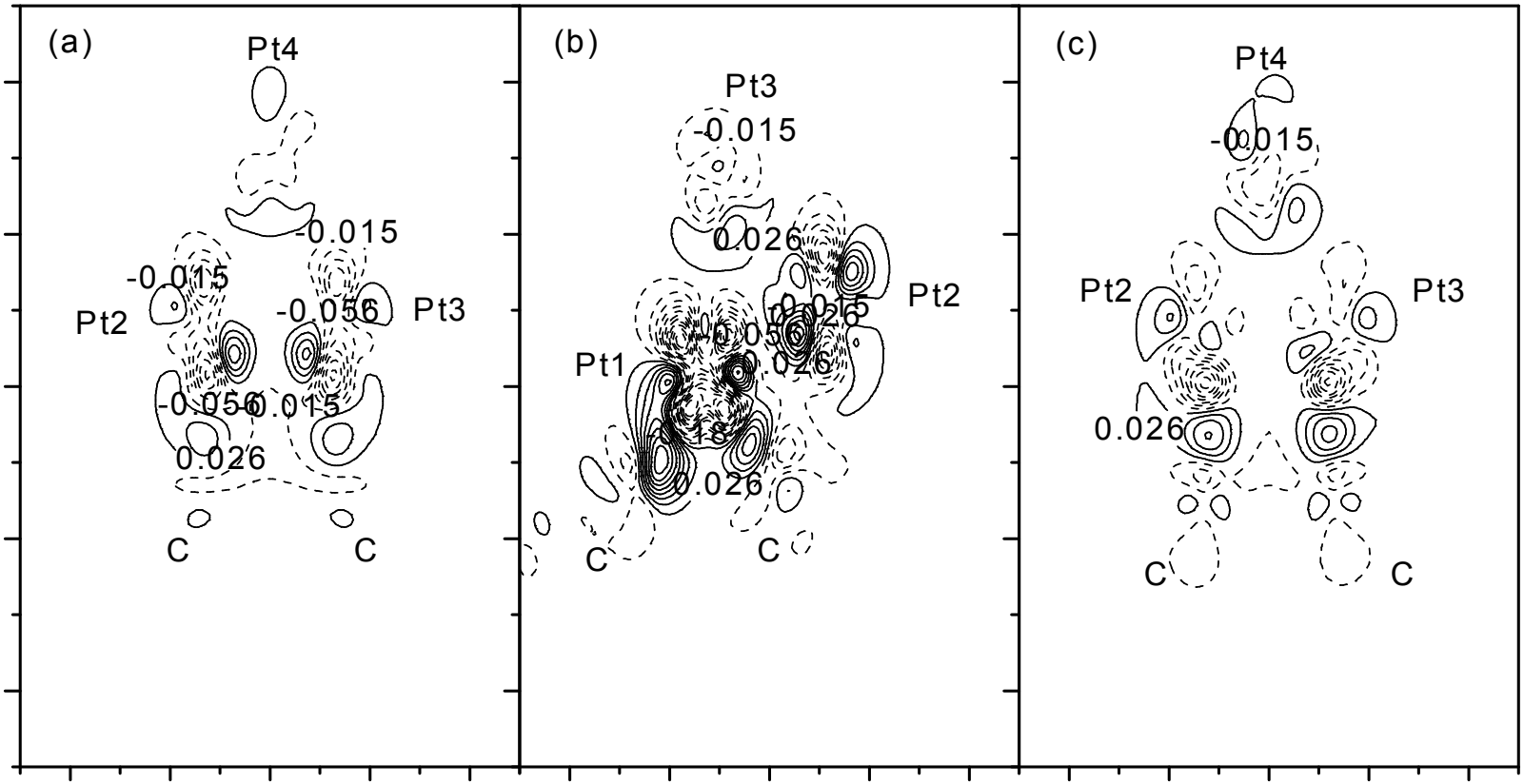

Fig. 3.

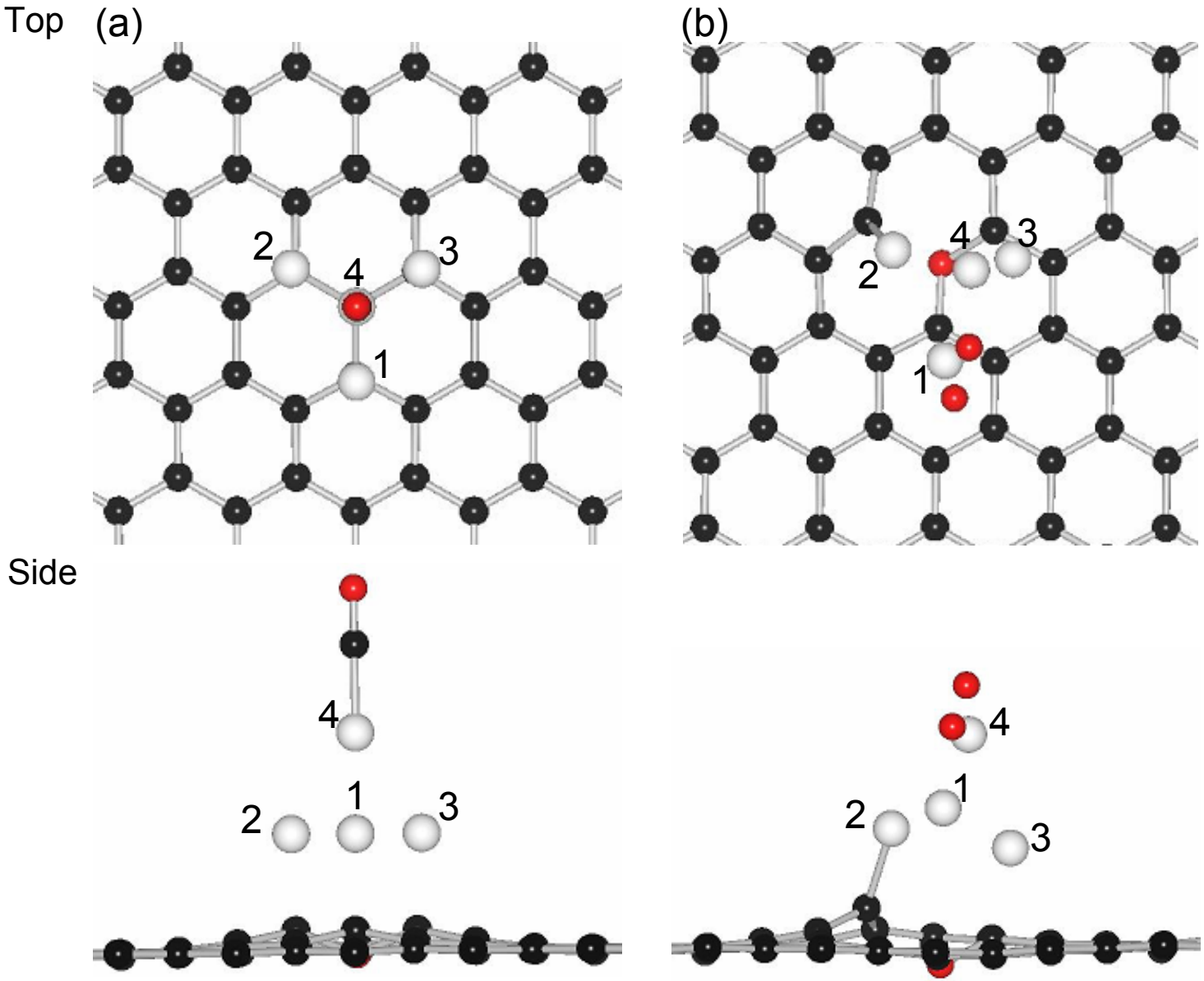

Fig. 4.

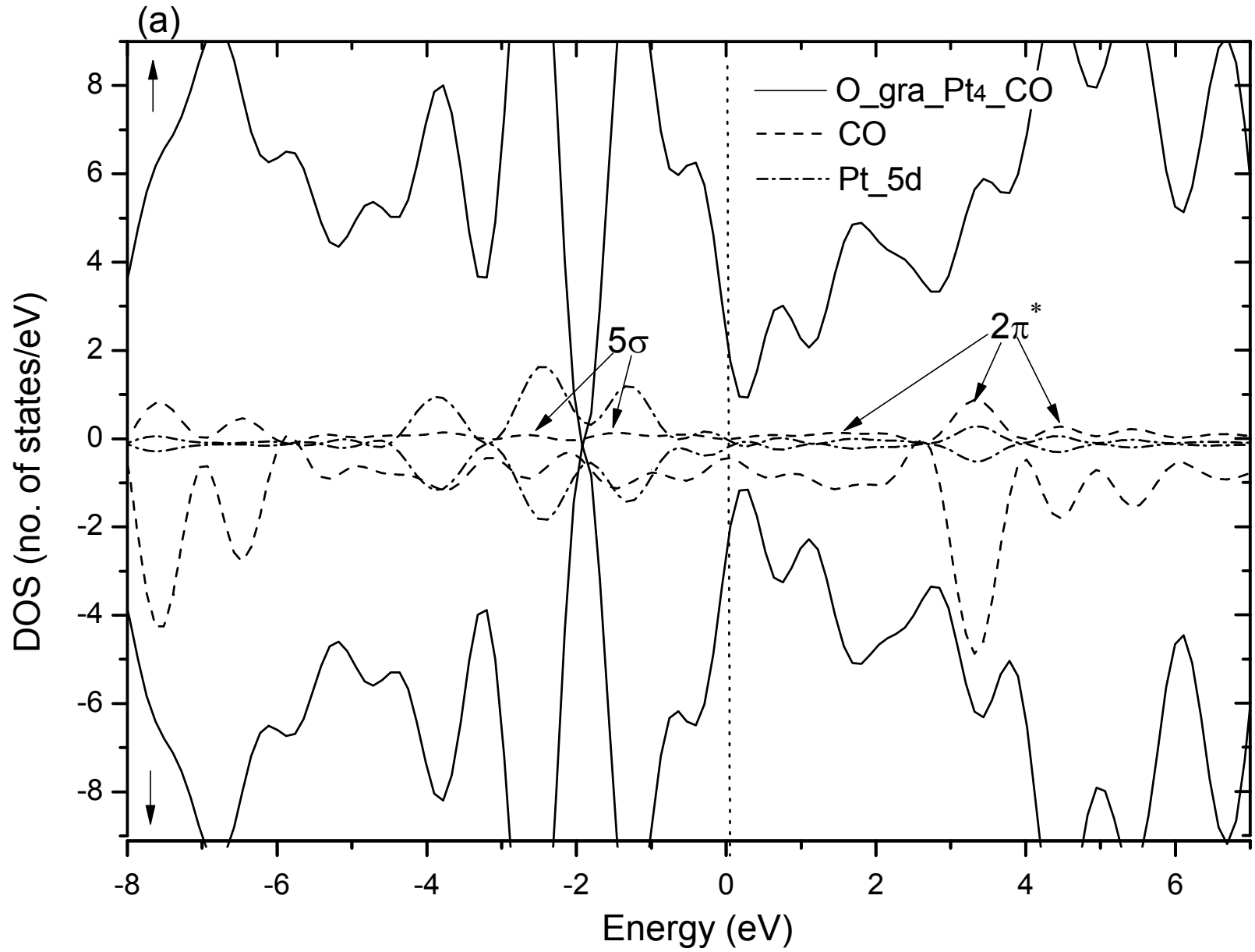

Fig. 5(a)

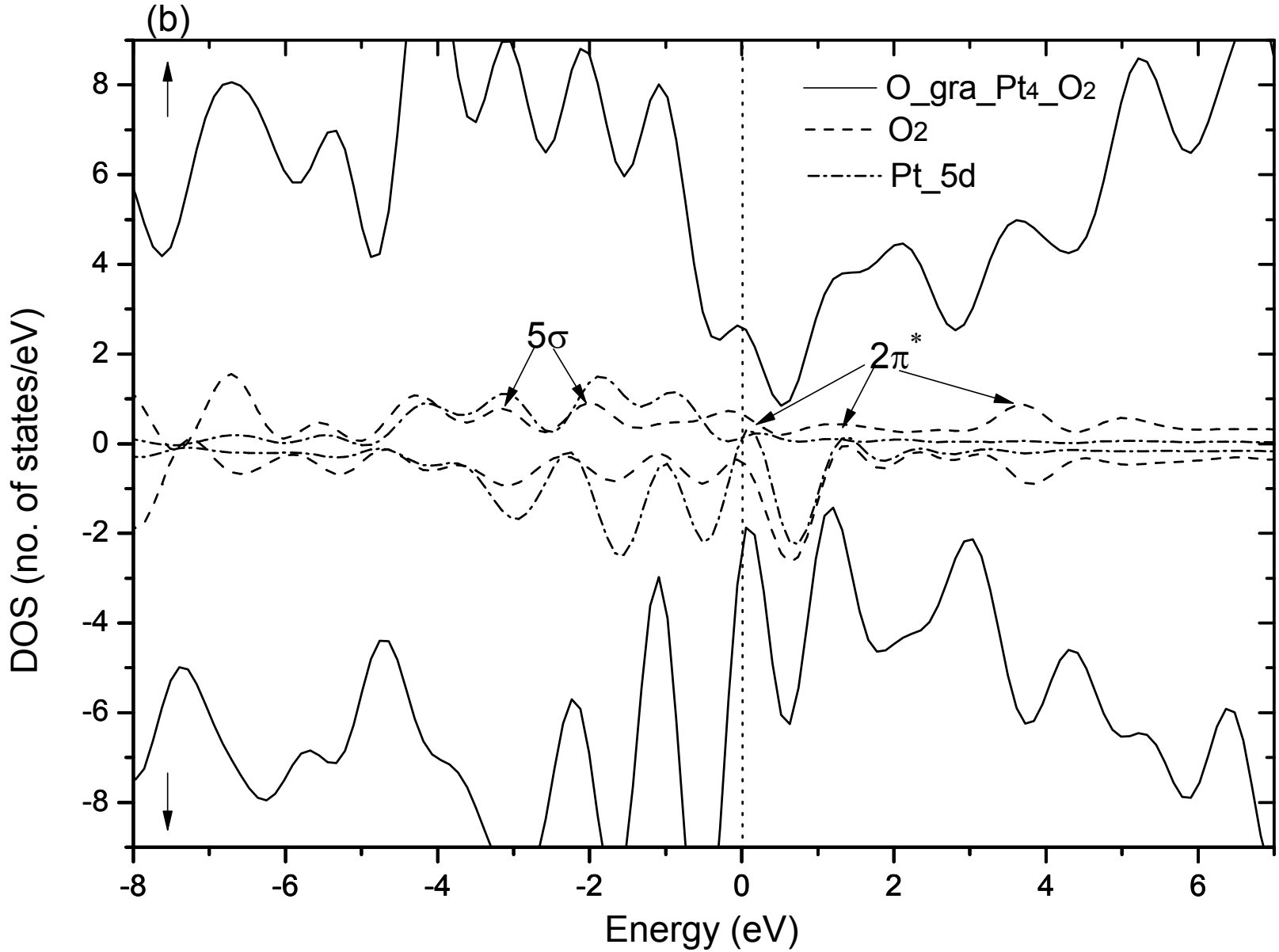

Fig. 5(b)

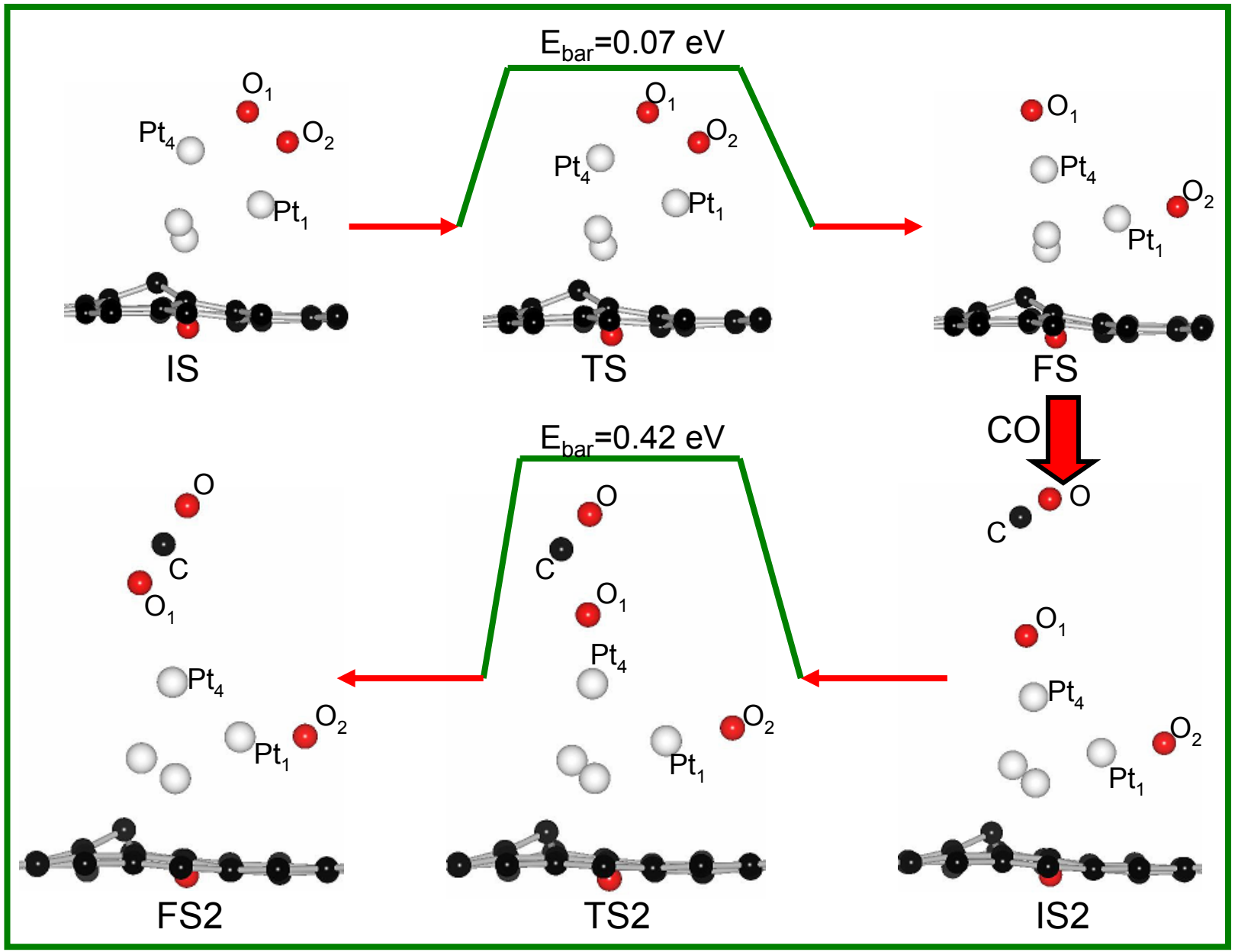

Fig. 6(a)

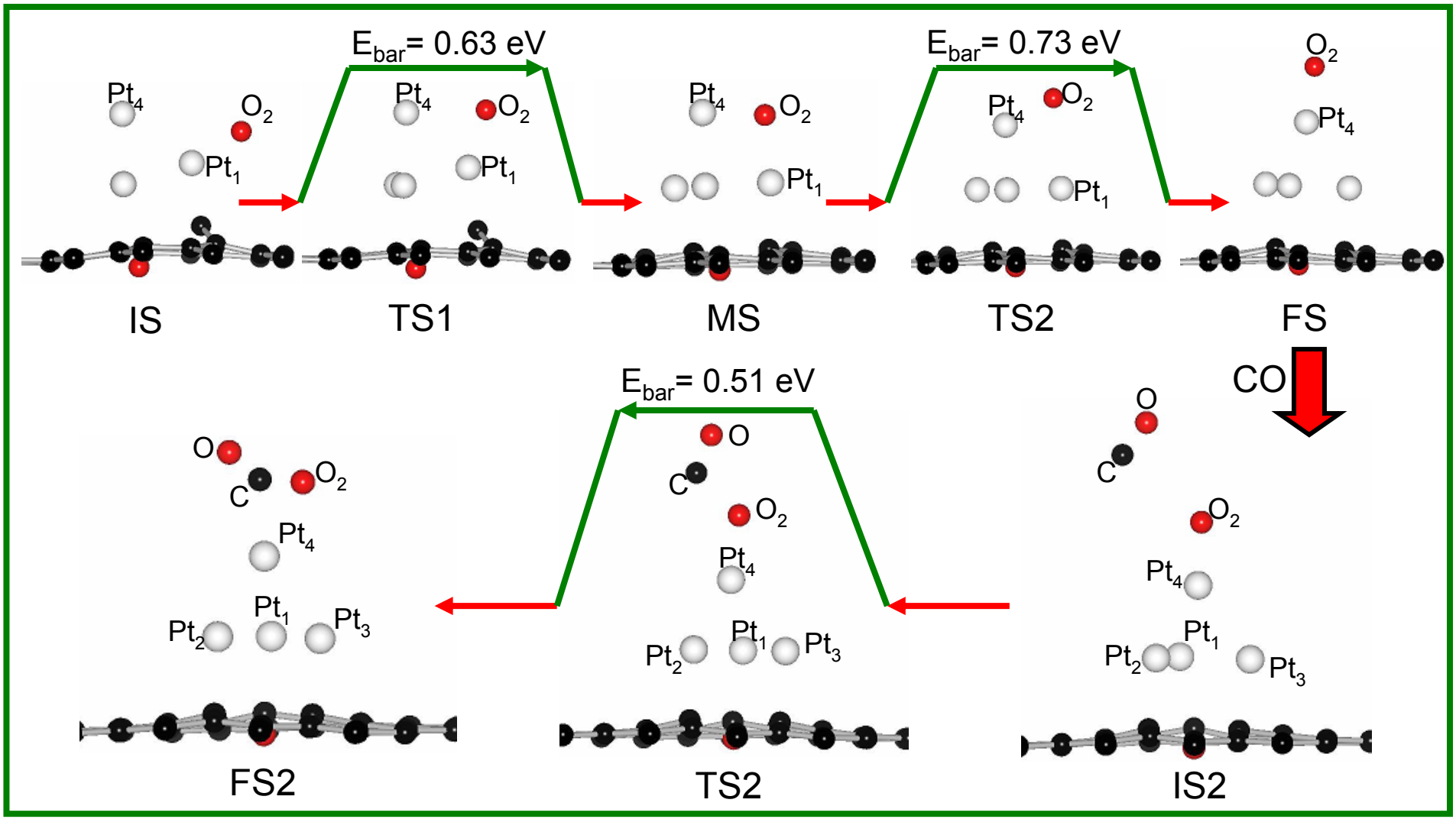

Fig. 6(b)

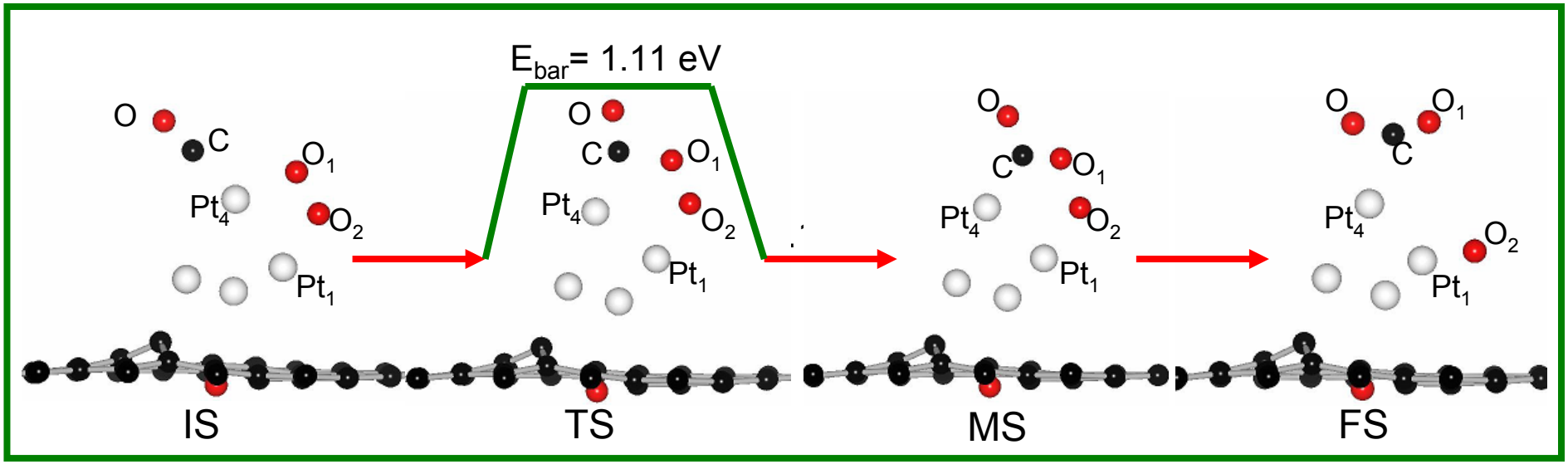

Fig. 6(c)